PHYSICAL/COMPUTATIONAL FRAMEWORK FOR EGS *IN SITU* FRACTURE STIMULATION

Justin Pogacnik[1], Peter Leary[1] and Peter Malin[1]

[1]Institute of Earth Science and Engineering, The University of Auckland, 58 Symonds Street, Auckland, New Zealand

j.pogacnik@auckland.ac.nz

Keywords: *Fully coupled finite element model, deformable porous media, Engineered/Enhanced Geothermal Systems, heat and mass transfer, permeability enhancement, power-law scaling.*

ABSTRACT

We employ a fully coupled finite element analysis of a thermal, hydraulic, and mechanical (THM) energy scheme to simulate stress/strain damage induced in an *in situ* poroperm medium stressed by wellbore fluid pressurization in the medium. Our poroperm medium is characterized by two empirical constraints: (i) a normally-populated fracture-density distribution that percolates fluid via long-range spatially correlated grain-scale fracture connectivity at all scale; and (ii) a (potentially) long-tailed ('lognormal') permeability distribution κ associated with percolation pathways related to normally distributed porosity distribution F expressed by $\kappa = \kappa_0 \exp(\alpha(\phi-\phi_0))$ as attested by clastic reservoir well-core poroperm fluctuation systematics. The degree of fracture connectivity in such a medium is parameterized by α = ratio of standard deviations of logκ and ϕ distributions. Small values of α describe low degrees of fracture connectivity and hence low bulk permeability, while large values of α describe high degrees of fracture connectivity giving high bulk permeability. Wellbore fluid pressurization creates shear strains in the fracture-heterogeneous poroperm medium, putatively generating grain-scale fracture damage additional to the pre-existing grain-scale fracture damage in the medium. Injecting grain-scale fracture damage can be seen as creating new fluid flow pathways and increased bulk permeability via newly created grain-scale fracture-connectivity. Pressure-induced fracture damage injection thus leads to greater fluid permeability equivalent to incrementing the value of the fracture-connectivity parameter α. Such wellbore pressurization could be conducted in interest of flow stimulation of an inter-wellbore EGS heat exchange volume.

1. INTRODUCTION

Traditionally, the true spatial variations of porosity and permeability are ignored in favor of their mean values (e.g., Sutter et al., 2011). However, previous work indicates that it is imperative to consider true spatial fluctuations in 'poroperm' properties. Leary and Walter (2008) show that observed tight gas well production unpredictability is traceable to the false assumption that *in situ* flow in gas sands is quasi-uniform rather than spatially fluctuating. On an economic note, Goldstein et al (2011) cite "insufficiently predictable reliability of geothermal reservoir performance (and in particular, the [un]predictable reliability of EGS reservoirs)" that is traceable to EGS models based on quasi-uniform media.

Quasi-uniform media are effectively assumed to have a 'white noise' Fourier power-spectra in spatial frequency *k*,

$$S(k) \sim const. \tag{1}$$

Microresistivity and most other geophysical well-log data have, however, Fourier power-spectra that scale inversely with wave number by

$$S(k) \sim \frac{1}{k} \tag{2}$$

over about 5 decades of the length scale from 10^{-2}m to 10^{3}m. Leary, *et al*. 2012 offers a detailed description of the empirical wellbore-based "rules" given in equations (2)-(4b). Equation (2) can be interpreted to mean that *in situ* fracture systems are spatially correlated grain-scale fracture density networks that fluids percolate through on all scale lengths. The specific well log properties that obey (2) include: sonic wave speeds, electrical resistivity, soluble chemical species density, neutron porosity, and mass density (Leary, 2002).

Clastic rock well-core data show a close spatial fluctuation relationship between well-core permeability κ and well-core porosity ϕ, via long-range fracture connectivity:

$$\delta\phi \sim \delta\log(\kappa) \tag{3}$$

where (3) can be interpreted to mean that porosity controls permeability through interconnectivity of grain-scale fracture networks that allow fluids to percolate. Leary and Walter (2008) offer a detailed description of (2) and (3). Their approach is different because, while the lognormal or 'long-tailed' trend in permeability and other well data have been noted for years, i.e., Law (1944) and Bennion & Griffiths (1966), there have been few reported attempts to understand the physics underlying long-tailed permeability distributions and the normal to lognormal transition in permeability and various ore grade and trace element distributions.

Leary, *et al*. 2012 offer a detailed description of the integration of (3) to yield:

$$\kappa = \kappa_0 \exp(\alpha\phi) \tag{4a}$$

where κ_0 and α parameters that can be determined from specific well-log and well-core data and

$$\alpha \equiv \frac{\sigma_{sd}(\log\kappa)}{\sigma_{sd}(\phi)} \tag{4b}$$

where σ_{sd} is the standard deviation of the well properties over the entire well. Since α is a factor in the exponential term of (4a), it controls the transition of the permeability distribution from normal to long-tailed. That is, low values of α result in a nearly normal distribution and high α values result in more lognormal-like distributions. Further, α has

been seen to fluctuate from about 2.5 to 30 in clastic rock systems analyzed by Leary, *et al.* 2012. The transition to long-tailed occurs due to an understandable physical reason in (4a) rather than being a function of arbitrary statistical parameters that govern lognormal distributions.

This work simulates subsurface fluid flow and heat transport within a 2-D deformable porous medium with power-law scaling fluctuations in porosity as per (2) combined with the aforementioned relationship controlling permeability (3)-(4b). We are most interested in simulating injection-induced permeability enhancement. Nathenson (1999) provides an overview of different permeability enhancement models and compares the results to Rosemanowes, Cornwall, UK, field data. The models are formulated in terms of effective stress, however, mechanical stress is assumed constant and the models become dependent only upon fluid pressure. In this work, we examine the inverse power relation from Nathenson's review. The model was originally calibrated by using the analytical well to well flow solution from De Wiest (1965) assuming flow through a uniform medium. Injection induced damage occurs as a result of mechanical deformation caused by injection pressurization. In this work, we seek to extend the inverse power relationship to include mechanical deformation effects.

Cladouhos, et al. (2009) propose that sustainable EGS requires controlled shear induced permeability enhancement termed *hydroshearing*. To that end, we use a poroperm medium that accounts for natural spatial fluctuations in permeability and porosity and analyze the medium for shear stress concentrations. We then assume that damage occurs in areas of high shear stress concentrations and effectively increases fracture connectivity, not fracture density. The methods and results of these analyses will be presented here.

2. EQUATIONS AND NUMERICS

2.1 Linear Momentum Balance

A suitable first step in acquiring the finite element system of equations is to consider the linear momentum balance:

$$\underline{\nabla} \cdot \underline{\underline{\sigma}} + \rho \underline{g} = \underline{0} \tag{5}$$

where $\underline{\nabla}\cdot$ refers to the gradient operator, $\underline{\underline{\sigma}}$ is the Cauchy stress tensor, $\underline{g}$ is the gravity acceleration vector, and ρ is the average density of the entire matrix:

$$\rho = (1-\phi)\rho^{s} + \phi\rho^{w}, \tag{6}$$

where ρ^{s} is the density of the solid grains, ρ^{w} is the density of the fluid (water) surrounding the grains, and ϕ is the porosity defined as the volume of void space per unit volume. The Cauchy stress can be expressed as a vector and split into two components, the effective stress component $\underline{\sigma}''$ and a pore pressure component as

$$\underline{\sigma} = \underline{\sigma}'' - \underline{m}p, \tag{7}$$

where $\underline{m}$ is related to the identity tensor, and p is the pore fluid pressure (Lewis and Schrefler 1998; Ingebritsen, Sanford, and Neuzil 2006). Assuming linear isotropic elastic behavior, the effective stress is calculated as

$$\underline{\sigma}'' = \underline{\underline{D}}_{e}\left(\underline{\varepsilon} - \underline{\varepsilon}_{T}\right), \tag{8}$$

where $\underline{\underline{D}}_{e}$ is the standard elasticity tensor, $\underline{\varepsilon}$ is the mechanical strain vector, and $\underline{\varepsilon}_{T}$ is the thermal strain vector. In the effective stress equation,

$$\underline{\varepsilon} = \underline{\underline{L}}\,\underline{u} \tag{9}$$

and

$$\underline{\varepsilon}_{T} = \underline{m}\left(\beta_{s}/3\right)T \tag{10}$$

where $\underline{\underline{L}}$ is a matrix of spatial derivatives, $\underline{u}$ is the displacement vector, $\underline{m}$ again is related to the identity matrix, β_s is the coefficient of thermal expansion of the solid matrix, and T is the temperature.

2.2 Mass Balance

Consideration of both the fluid and solid mass balance equations gives:

$$\begin{aligned} 0 = &-\left((1-\phi)\beta_{s} + \phi\beta_{w}\right)\frac{\partial T}{\partial t} \\ &+\left(\frac{1-\phi}{K_{s}} + \frac{\phi}{K_{w}}\right)\frac{\partial p}{\partial t} + \underline{\nabla}\cdot\underline{v}^{s} \\ &+\underline{\nabla}\cdot\left\{\frac{\underline{\underline{\kappa}}}{\mu_{w}}\left[-\underline{\nabla}p + \rho g\right]\right\} - Q_{p} \end{aligned} \tag{11}$$

where S_w is the fluid saturation and has been omitted for the fully saturated case, $\underline{v}_{s}$ is the solid matrix velocity from the system elastic modulus, $\underline{\underline{\kappa}}$ is the permeability matrix, and Q_p is fluid flow into the system.

2.3 Energy Balance

Lastly, to fully couple thermal effects, we consider the enthalpy balance equation:

$$\begin{aligned} 0 = &\left(\rho_{w}C_{w} + C_{s}\rho_{s}\right)\frac{\partial T}{\partial t} \\ &+\rho^{w}C_{w}\frac{\underline{\underline{\kappa}}}{\mu_{w}}\left(-\underline{\nabla}P + \rho\underline{g}\right)\cdot\underline{\nabla}T - \underline{\nabla}\cdot\left\{\underline{\underline{\chi}}\cdot\underline{\nabla}T\right\} \end{aligned} \tag{12}$$

where C_w is the specific heat of the fluid, C_s is the specific heat of the solid grains, and $\underline{\underline{\chi}}$ is related to the diffusivity of the medium.

The thermal properties of solid are taken to be constant in space and time (rock thermal properties vary only slightly, Clauser and Huenges 1995). Fluid density and fluid viscosity were taken to have the temperature dependence as prescribed by Likhachev (2003). The temperature

dependent equation is valid up to about 250°C as long as the fluid does not undergo a phase change. Likhachev also formulates the pressure dependence of these parameters, but the effects are small and have been ignored here. The possibility does exist, however, to incorporate the pressure dependence.

2.4 The Finite Element Method

Figure 1 depicts an arbitrary 2-D porous domain Ω with a boundary Γ that is subject to natural and essential boundary conditions on portions of Γ denoted Γ_h and Γ_g, respectively. Natural boundary conditions enforce forces on the system, such as external tractions, mass fluid flow, or temperature fluxes. Essential boundary conditions enforce known degrees of freedom, such as solid displacements, pore fluid pressures, and temperature. The domain is considered to be a fully saturated assemblage of rigid solid grains bonded by weak cements and having a spatially fluctuating density of fluid-filled void space between grains. Void space fluids percolate between voids where grain-grain cement bonds are ruptured by tectonically imposed finite-strain of the bulk medium. The controlling physical variable is grain-scale fracture density. At a critical density of grain-scale fractures, long-range spatial correlations between grain-scale fractures arise, creating the observed power-law scaling properties of well log spatial fluctuations (Leary 2002; Leary *et al.* 2012).

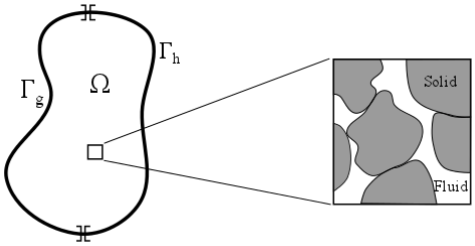

Figure 1. An arbitrary porous domain in a poroperm medium comprising void fluids (white) and solid grains (dark) that may or may not be bonded by intact cements. Void-to-void percolation of fluid is assumed to occur where grain cements are naturally disrupted by finite-strain dislocations due to tectonic processes, or in the present example by high pressure fluids introduced via a wellbore in the medium. The presence/absence of cement bonds/disruption is assumed to be highly spatially erratic and heterogeneous at all scale lengths throughout the medium; there is no assumed 'effective medium' or 'continuum' approximation.

The solid-fluid matrix is non-isothermal and grain assemblages are subject to small strains on all scale lengths. Therefore, the problem is evaluated as a coupled problem involving temperature and fluid flow through a deformable porous medium.

The details of the finite element discretization used here can be found in Pogacnik (2012) and are adapted from the well-established procedures found in Lewis and Schrefler (1998) and Zienkiewicz and Taylor (2000). The final matrix system of equations takes the form (13):

$$\begin{bmatrix} \underline{\underline{K}} & -\underline{\underline{Q}} & \underline{\underline{K}}_{tt} \\ \underline{\underline{0}} & \underline{\underline{H}} & \underline{\underline{0}} \\ \underline{\underline{0}} & \underline{\underline{0}} & \underline{\underline{K}}_{t} \end{bmatrix} \begin{Bmatrix} \underline{u} \\ \underline{p} \\ \underline{T} \end{Bmatrix} + \begin{bmatrix} \underline{\underline{0}} & \underline{\underline{0}} & \underline{\underline{0}} \\ \underline{\underline{Q}}^T & \underline{\underline{S}} & \underline{\underline{R}} \\ \underline{\underline{0}} & \underline{\underline{0}} & \underline{\underline{C}}_{t} \end{bmatrix} \frac{d}{dt} \begin{Bmatrix} \underline{u} \\ \underline{p} \\ \underline{T} \end{Bmatrix} = \begin{Bmatrix} \underline{f}_u \\ \underline{f}_p \\ \underline{f}_t \end{Bmatrix}$$

where the unknowns are the nodal solid displacements ($\underline{u}$), pore fluid pressures ($\underline{p}$), and temperatures ($\underline{T}$). This system can be re-written as

$$\underline{\underline{A}}\,\underline{x} + \underline{\underline{B}}\frac{d\underline{x}}{dt} = \underline{F} \qquad (14)$$

and is solved using a single-step finite difference operator in the standard way.

In this paper, we consider 2D sections of earth in two perpendicular directions to approximate well to well flow scenarios. In general, the boundary pressure is equivalent to the pressure and depth. Roller boundary conditions are places on the outside walls of the domain that constrain deformation in the normal direction. An injection well incurs over pressurization and receiver wells are held constant at the depth pressure. In the present case, the fluid temperatures are everywhere at ambient rock temperature; omitting thermal effects simplifies the interpretation of computed strain. The material parameters specified in the model that were used in this paper are given in Table 1.

Table 1. Material Input Parameters

Parameter	Symbol	Value	Units
Young's modulus	E	7.2000E+10	Pa
Poisson's ratio	ν	0.14	-
fluid density	ρ^w	1000	kg/m^3
solid density	ρ^s	2600	kg/m^3
mean porosity	□	1.10E-01	-
permeability	κ_0	1.31E-15	m^2
fluid viscosity	μ_w	1.20E-04	kg/(m s)
fluid bulk modulus	K_f	2.20E+09	Pa
solid coefficient of thermal expansion	β_s	5.50E-07	1/°C
fluid coefficient of thermal expansion	β_w	2.02E-04	1/°C
solid specific heat	C_s	840	J/(kg °C)
fluid specific heat	C_w	4187	J/(kg °C)
solid thermal conductivity	α_s	3.5	J/(s m °C)
fluid thermal conducitivity	α_w	0.6	J/(s m °C)

3. PERMEABILITY ENHANCEMENT

Nathenson (1999) provides an overview of a few different permeability enhancement relationships (inverse power, cubic power, cubic-log, and exponential) based on effective stress (σ - p). He uses a simple 1-D well to well flow analytical solution with optimized material parameters to match field data taken from the Rosemanowes, UK, geothermal field. The enhancement relation favored in Nathenson's analysis was the inverse power relationship given by:

$$\kappa = \frac{\kappa_0}{\frac{1}{\sigma_c}(\sigma - p)} \qquad (15)$$

where κ_0 is baseline permeability, σ_c is the confining stress (taken to be the horizontal confining stress), σ is the Cauchy stress, and p is the pressure. Nathenson states that it is reasonable to assume $\sigma = \sigma_c$ at depth. Therefore, the expression takes the form:

$$\kappa = \frac{\kappa_0}{\left(1 - \frac{p}{\sigma_c}\right)} \tag{16}$$

This form of the inverse power relation has been implemented in our finite element code in 2-D where σ_c is taken to be a constant that is equal in either coordinate direction x or y.

In order to extend Nathenson's work to a more general case in higher dimsions, we formulate equation (15) in terms of the full stress tensor with potentially variable initial principle stress components in the *in situ* stress state, which would now be expressed as a second order tensor. A more general form of equation (15) could be written as

$$\underline{\underline{\kappa}} = \underline{\underline{\kappa}}_0 \left\{ \left[\underline{\underline{\sigma}} - p\underline{\underline{I}} \right] \underline{\underline{\sigma}}_c^{-1} \right\}^{-1} \tag{17}$$

where, in 2-D,

$$\underline{\underline{\kappa}}_0 = \begin{bmatrix} \kappa_0 & 0 \\ 0 & \kappa_0 \end{bmatrix} \tag{18}$$

$$\underline{\underline{\sigma}} = \begin{bmatrix} \sigma_{xx} & \sigma_{xy} \\ \sigma_{xy} & \sigma_{yy} \end{bmatrix} \tag{19}$$

$$\underline{\underline{\sigma}}_c = \begin{bmatrix} \sigma_h & 0 \\ 0 & \sigma_v \end{bmatrix} \tag{20}$$

where σ_h and σ_v are the horizontal and vertical components of the *in situ* stress state. σ_h is taken to be the same thing as σ_c in equation (15). Nathenson's inverse power relation obviously breaks down when the confining stress and pressure are equal since the permeability approaches infinity. However, this case could correspond to a hydrofracking scenario and represents a change in failure mode from shear failure to normal crack opening. This is exactly the case that should be avoided in EGS since hydrofractured "super-hiways" can allow cold fluid to pass from well to well.

In order to further ellucidate the effects that mechanical deformation may have on the permeability in Nathenson's formulation, a third case was set up in which only mechanical stress effects were considered:

$$\underline{\underline{\kappa}} = \underline{\underline{\kappa}}_0 \left\{ \left[\underline{\underline{\sigma}} \right] \underline{\underline{\sigma}}_c^{-1} \right\}^{-1} \tag{21}$$

In our analyses, it has become apparent that geometry and boundary conditions play a significant role in the stress state reponse of the medium. In addition to the above formulations given in equations (16), (17), and (21), a fourth permeability enhancement option was considered where permeability is increased in areas of shear strain concentration. The shear strain concentrations are caused by injection well overpressurization resulting in fluid percolating through natural pathways in the medium. We propose that shear strain concentrations result in an increase in existing fracture connectivity, α, from equation (4). For a first approximation, we take the isotropic permeability to increase with increased fracture connectivity following (4) as:

$$\kappa = \kappa_0 \exp\left\{ \left(\alpha + \alpha^* \frac{\varepsilon_{xy}}{\varepsilon_{xy}^{\max}} \right) \left(\phi - \phi_0 \right) \right\} \tag{22}$$

where α^* is the fracture connectivity stimulation factor, ε_{xy} is the shear strain at a point, $\varepsilon_{xy}^{\max}$ is the maximum shear strain in the entire domain, and ϕ_0 is the minimum pososity (taken to be fracture porosity) in the domain. Therefore the shear strain at a point is normalized by the maximum shear strain in the domain. This is a first order approximation to a method for enhanced permeability through shear strain induced damage. Normalizing the shear strains helps to visualize areas of shear strain concentration in the domain. Validating and refining the model is the subject of future work.

4. NUMERICAL RESULTS AND DISCUSSION

4.1 Uniform Media

For the inverse power relation, the same material parameters presented by Nathenson were used here and are presented in Table 2.

Table 2. Inverse power material parameters from Nathenson (1999)

Parameter	Symbol	Value	Units
initial permeability	κ_0	1.31E-15	m^2
horizontal confining stress	σ_h	3.35E+07	Pa
vertical confining stress	σ_v	5.40E+07	Pa

Nathenson provides data from Rosemanowes wells RH12 (injection) and RH15 (receiver) with which to compare permeability enhancement relations. The general set up is given by two parallel wells that are 150 m apart in horizontal distance with an average of 275 m of open-hole well each. Nathenson states that the open-hole portions of the wells are offset by 400 m of vertical distance and scales permeability by an unspecified "adjustment." He explains that the adjustment affects the baseline permeability (κ_0) but not the function dependence of permeability on pressure. Figure 2 (left) displays the finite element mesh used to represent the Rosemanowes scenario. Figure 2 (right) displays the enhanced permeability repsonse using equation (16) and Figure 3 (left) displays the stress state between the wells and (right) displays the enhanced permeability as calculated by equation (21).

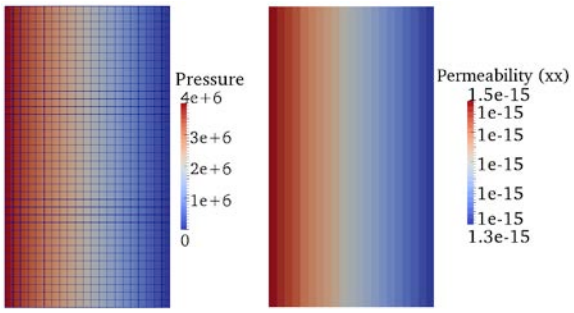

Figure 2. Finite element mesh with the pressure result (Left) and the enhanced permeability result (Right) to represent the Rosemanowes site data constructed from specifications found in Nathenson (1999). The left side of the mesh represents the injection well and the right side the receiver well. The pressure differential between the wells is 40 bars. The horizontal distance between the wells is 150 m and the open-hole height is 275 m. The initial permeability was uniformly set to 1.31E-15 m^2. Permeability was enhanced by the pressure-dependent equation (16).

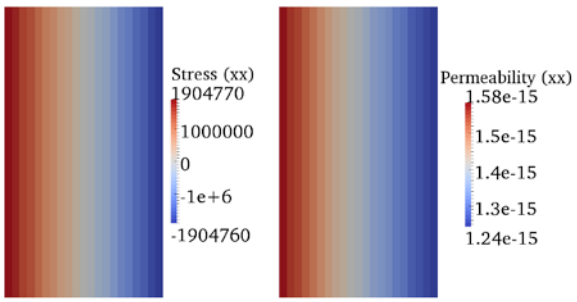

Figure 3. Response for horizontal component of stress tensor, σ_{xx} (left), and enhanced permeability, κ_{xx} (right), for permeability enhancement controlled by equation (21). The areas of compression result in an effective reduction in permeability, while tensile stress results in permeability enhancement.

Permeability enhancement ultimately affects the percolation flow through a porous medium. Figure 4 shows the average flow results from the Rosemanowes wells and the results for each different use of the inverse power permeability enhancement equation.

Figure 5 displays the flow results for a vertical slice through three-spot horizontal well bore set up. The center well is overpressurized to 8 MPa over the initial hydrostatic pressure. The two receiver wells are situated on either side of the injector well and are fixed at hydrostatic pressure. The figure also displays the horizontal component of the mechanical stress tensor (middle) and the final enhanced permeability result (bottom).

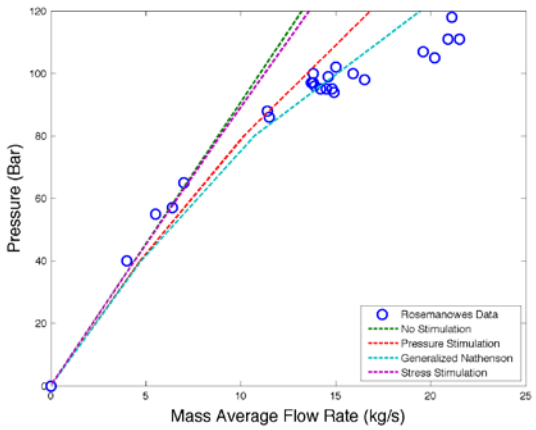

Figure 4. Rosemanowes average flow data compared to simulation results for no permeabilty enhancement and the different forms of permeability enhancement derived from the inverse power law presented in Nathenson (1999). Permeability enhancement results in higher fluid velocities and higher flowrates at equivalent pressure drops between wells.

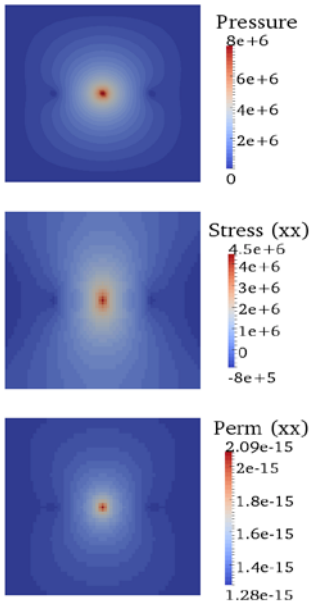

Figure 5. Three-spot horizontal well bore simulation result for pressure in Pa (top), horizontal component of mechanical stress in Pa (middle), and horizontal component of enhanced permeability in m^2 (bottom). Enhanced permeability was computed using equation (17) and is a function of effective stress. The initial permeability was uniformly set to 1.31E-15 m^2.

4.2 Poroperm Medium

The previous section relies on the assumption that initial permeability is uniform in the medium. A poroperm medium was constructed that adheres to the empirical constraints of equations (2), (3), and (4). Figure (6) displays the poroperm medium with spatially fluctuating porosity and permeability values. Permeability enhancement occurs as a result of injection pressure, stress state, and/or shear strain induced damage. So far, only injection over pressure

values of 2 MPa were used in the investigation of permeability enhancement in the poroperm medium.

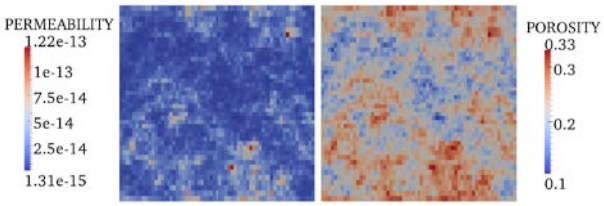

Figure 6. Poroperm medium used with realistic spatial fluctuations in permeabilty in m^2 (left) and porosity (right). Small changes in porosity result in large changes in permeability. The total flucutation in porosity is 0.13 but permeability fluctuates nearly 2 orders of magnitude.

Figure 7 displays the well to well flow geometry where injection stimulation was induced by shear strain concentrations as in equation (22). Figure 8 displays the fluid velocities to visualize how fluids percolate through the poroperm medium. Table 3 displays the flow results for horizontal flow through the medium with both the stress/pressure dependent inverse power rule of equation (17) and with the shear strain concentration induced fracture connectivity enhancment method. A 2 Mpa over pressurization induces shear strain damage that increases fluid throughput by about 10% from the zero stimulation case (1.94 kg/s to 2.13 kg/s).

A curious result of the inverse power method is that the inflow value is higher than the outflow. A possible physical explanation for this phenomenon lies in the fact that the flow calculations are made along the parallel vertical edges. The left edge (inflow) has high pressurization of the injection well acting on its surface to effectively reduce the compressive stress and increase permeability, while the right edge (outflow) has increased compressive stress acting on it due to the the pressure from the left hand well. The increased compressive stress acts to reduce permeability and divert fluids away from the receiver well. The enhanced permeability is no longer isotropic because the inverse power relationship uses the full stress tensor, the individual components of the permeability tensor can be affected, i.e., xx, xy, yy, and yx.

An encouraging result of the shear strain induced damage relationship when applied to a poroperm medium is that damage is high in areas where natural percolation pathways exist. In Figure 7, notice the high shear strain concentrations in the bottom right-hand portion of the domain. The fluid velocity plot from Figure 8 shows that the highly strained area is also where fluid velocity and flow is the greatest. This area is then damaged the most and flow is increased even more in the area with initially high fracture connectivity. This is consistent with reported results from the Rosemanowes site by Tester, *et al.* (2006). They state that it is possible to stimulate natural fractures for improved permeability. Figures 7 and 8 do show this type of phenomenon. Further, this can easily lead to the short-circuit case mentioned by Tester, *et al.* (2006) where too much of the injection fluid passes through to the receiver well too quickly without sufficient time to gather heat energy.

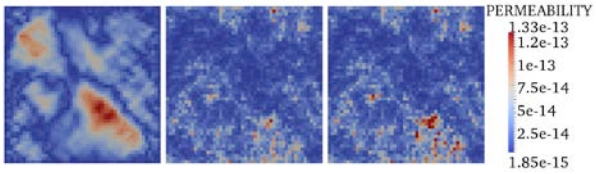

Figure 7. Permeability enhancement by fracture connectivity increases due to shear strain concentrations in the medium. Fluid flows from left to right through the medium. The left image displays shear strain concentrations that result from fluid percolating through native permeability pathways in the rock that can be seen in Figure 8. The fracture connectivity parameter α was then increased in areas of high shear strain concentrations. The center image displays the initial permeability field and the right image shows the enhanced permeability field. The maximum permeability increased from 1.22E-13 to 1.33E-13 m^2.

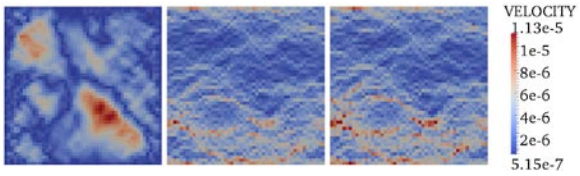

Figure 8. Fluid velocities in m/s for horizontal flow in the poroperm medium. The left image displays the shear strain concentrations, the center image displays the fluid velocity through unenhanced pathways, and the right image displays fluid velocity with strain-induced enhancement in fracture connectivity.

Table 3. Comparison of inflow and outflow rates for horizontal well to well flow with different stimulation rules.

Stimulation Rule	Inflow (kg/s)	Outflow (kg/s)
No Stimulation	1.94	1.94
Inverse Power	2.12	1.89
Shear Strain Induced Damage	2.13	2.13

Permeability enhancement simulations were run on the three spot well bore geometry seen in Figure 5 with the poroperm medium description. The flow results for the injection and receiver wells can be seen in Table 4. Similarly, to Table 3, increases in compression around receiver wells result in decreased permeability around those wells. Hence, the slight reduction in outflow with the inverse power rule for stimulation. Figure 9 displays the shear strain concentrations around the injection well that result from fluids percolating through natural permeability channels in the poroperm medium. The results seem to indicate that induced damage increases input well flow but the effect does not carry to the output well. We learn from this that (i) both input and output wells need stimulation, and (ii) near-well fracture stimulation will have to be large to permit stimulation effects away from the well.

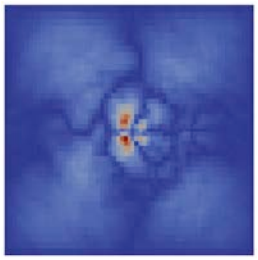

Figure 9. Normalized shear strain concentrations around a three spot wellbore geometry within a poroperm medium. The shear strain concentrations lead to increase in fracture connectivity, which in turn increases permeability.

Table 4. Comparison of inflow and outflow rates for three spot well bore simulations with different stimulation rules.

Stimulation Rule	Inflow (kg/s)	Outflow 1 (kg/s)	Outflow 2 (kg/s)
No Stimulation	2.14	0.38	0.46
Inverse Power	2.28	0.38	0.46
Shear Strain Induced Damage	2.33	0.4	0.51

5. CONCLUSIONS AND FUTURE WORK

It is clear that the physical processes that control permeability evolution in EGS volumes are not known. Past literature provides potential relations that could be used, but it the physical basis of these relationships is unclear. Further, past relationships, such as the inverse power rule, do not naturally account for damage that may occur in the medium. We propose a method that utilizes shear strain concentrations where fracture damage and fracture connectivity will increase. When applied to a poroperm medium with realistic spatial fluctuations in porosity and permeability, the strain induced damage method is able to show fracture stimulation that is qualitatively similar to the behavior reported at the Rosemanowes EGS site. Iis highly desirable to obtain injection/receiver flow data and porosity/permeability data from an EGS site, such as Rosemanowes, to test the validity of the shear strain induced damage model in a more quanitative way.

A major limiting factor however, is that the exact physics and relationships that govern the permeability increase still remain unclear. Further, our work has been limited to small strain elastic behavior. It is imperitive to extend this work to include irreversible deformations, such as plasticity and/or damage. Figure 10 displays the Von Mises yield criterion (J_2) result for the three spot well bore problem calculated as outlined in Chen and Han (1995). Areas of high principal stress differentials would be subject to irreversible deformations such as damage or plasticity. It will be important to consider the effects that a heterogenous, potentially, non-isotropic medium have on the irreversible damage in future analyses.

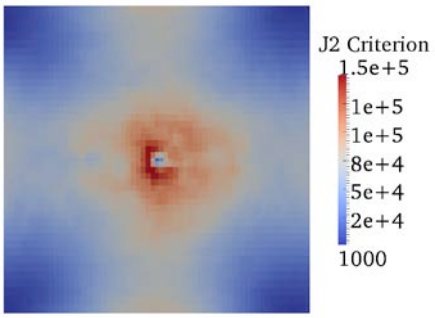

Figure 10. Von Mises J_2 yield criterion around the three spot well bore setup. Areas that surpass a J_2 yield criterion could be subject to a different bulk constitutive behavior that may include plasticity and/or damage.

ACKNOWLEDGEMENTS

The authors would like to acknowledge Dr. Rob Podgorney of Idaho National Laboratories and David Dempsey of The University of Auckland for their helpful discussions related to this work.

REFERENCES

Bennion D and Griffiths J (1966). "A Stochastic Model for Predicting Variations in Reservoir Rock Properties." Society of Petroleum Engineers Journal, pp. 9-16.

Chen, W.F. and Han, D.J. (1995) "Plasticity for Structural Engineers." Gau Lih Boook Co. Ltd.

Cladouhos, T., Petty, S., Larson, B., Iovenitti, J., Livesay, B., and Baria, R. "Toward More Efficient Heat Mining: A Planned Enhanced Geothermal System Demonstration Project." Geothermal Resources Council Transactions, Vol 33. 2009.

Clauser, C. and Huenges, E. "Thermal Conductivity in Rocks and Minerals", Rock Physics and Phase Relations, A Handbook of Physical Constants, AGU Reference Shelf 3, 1995.

Goldstein, B.A., Hiriart, G., Tester, J., B., Bertani, R., Bromley, Gutierrez-Negrin, L.,C.J., Huenges, E., H, Ragnarsson, A., Mongillo, M.A. Muraoka, and V. I. Zui, (2011) "Great expectations for geothermal energy to 2100." Proceedings Thirty-Sixth Workshop on Geothermal Reservoir Engineering, Stanford University

Hughes, T.J.R. (2000) "The Finite Element Method: Linear Static and Dynamic Finite Element Analysis." Dover Publications.

Ingebritsen, S., Sanford, W., and Neuzil, C. (2006) "Groundwater in Geologial Processes." Cambridge University Press.

Law, J. (1944) "A Statistical Approach to the Interstitial Heterogeneity of Sand Reservoirs" Society of Petroleum Engineers Journal. pp 202-222.

Leary, P.C. Fractures and physical heterogeneity in crustal rock, in *Heterogeneity of the Crust and Upper Mantle – Nature, Scaling and Seismic Properties*, J. A. Goff,

& K. Holliger (eds.), Kluwer Academic/Plenum Publishers, NewYork, 155-186, (2002) .

Leary, P.C., Pogacnik, J.A., Malin, P.E. (2012). "Fractures ~ Porosity -> Connectivity ~ Permeability -> EGS Flow Stimulation." Geothermal Resources Council Transactions, Vol 36. 2012.

Leary, P.C. and Walter, L.A.: Crosswell Seismic Applications to Highly Heterogenous Tight Gas Reservoirs. *First Break* 26 (2008).

Lewis, R.W. and Schrefler, B.A. (1998). "The Finite Element Method in the Static and Dynamic Deformation and Consolidation of Porous Media." John Wiley and Sons. pp. 9 - 97, 341 - 394.

Likhachev, E.R. (2003). "Dependence of Water Viscosity on Temperature and Pressure." Technical Physics 48(4) 514-515.

Nathenson, Manuel (1999). "The Dependence of Permeability on Effective Stress from Flow Tests at Hot Dry Rock Reservoirs at Rosemanowes (Cornwall) and Fenton Hill (New Mexico)" *Geothermics* 28. pp. 315-340.

Pogacnik, J., Podgorney, R., and Leary, P. (2012). "Computational EGS: Modelling Fully-Coupled Heat and Fluid Flow Through a Deformable Fracture-Permeable Medium with the Finite Element Method." 2012 Conference of the Engineering Mechanics Institute. Notre Dame, Indiana.

Sutter, D., Fox, D.B., Anderson B.J., Koch. D.L., Rudolf von Rohr, P., Tester, J.W. (2011), "Sustainable heat farming of geothermal systems: a case study of heat extraction and thermal recovery in a model EGS fractured reservoir." Proceedings Thirty-Sixth Workshop on Geothermal Reservoir Engineering, Stanford University.

Tester, *et al.* (2006). *The Future of Geothermal Energy.* A Massachusetts Institute of Technology report. http://geothermal.inel.gov/publications/future_of_geothermal_energy.pdf

Zienkiewicz OC & Taylor RL (2000) *The Finite Element Method: Volume 1 – The Basis*, 5th Ed. Butterworth and Heinemann.